Imaging geochemical heterogeneities using inverse reactive transport modeling: An example relevant for characterizing arsenic mobilization and distribution

Fakhreddine, Sarah; Lee, Jonghyun; Kitanidis, Peter K.; Fendorf, Scott; Rolle, Massimo

Published in:
Advances in Water Resources

Link to article, DOI:
10.1016/j.advwatres.2015.12.005

Publication date:
2016

Document Version
Peer reviewed version

This is a Post Print of the article published on line 11th December 2015 and printed February 2016 in Advances in Water Resources, 88, 186-197. The publishers' version is available at the permanent link: doi:10.1016/j.advwatres.2015.12.005

Imaging geochemical heterogeneities using inverse reactive transport modeling: An example relevant for characterizing arsenic mobilization and distribution

Sarah Fakhreddine[1,*], Jonghyun Lee[2,*,#], Peter K. Kitanidis[2], Scott Fendorf[1], Massimo Rolle[3]

[1]Department of Earth System Science, Stanford University, Stanford, CA 94305, USA

[2]Department of Civil and Environmental Engineering, Stanford University, Stanford, CA 94305, USA

[3]Department of Environmental Engineering, Technical University of Denmark, 2800 Kgs. Lyngby, Denmark

* these authors contributed equally to this work

corresponding author : jonghyun@stanford.edu

Highlights

- Approach to estimate the spatial distribution of reactive minerals in the subsurface.
- Multi-scale applications for As-bearing pyrite distribution using oxygen measurements.
- Computationally efficient inversion coupling flow and multi-species reactive transport.
- As-bearing pyrite distributions characterized successfully with PCGA inverse modeling.

Abstract

The spatial distribution of reactive minerals in the subsurface is often a primary factor controlling the fate and transport of contaminants in groundwater systems. However, direct measurement and estimation of heterogeneously distributed minerals are often costly and difficult to obtain. While previous studies have shown the utility of using hydrologic measurements combined with inverse modeling techniques for tomography of physical properties including hydraulic conductivity, these methods have seldom been used to image reactive geochemical heterogeneities. In this study, we focus on As-bearing reactive minerals as aquifer contaminants. We use synthetic applications to demonstrate the ability of inverse modeling techniques combined with mechanistic reactive transport models to image reactive mineral lenses in the subsurface and quantify estimation error using indirect, commonly measured groundwater parameters. Specifically, we simulate the mobilization of arsenic via kinetic oxidative dissolution of As-bearing pyrite due to dissolved oxygen in the ambient groundwater, which is an important mechanism for arsenic release in groundwater both under natural conditions and engineering applications such as managed aquifer recharge and recovery operations. The modeling investigation is carried out at various scales and considers different flow-through domains including (i) a 1D lab-scale column (80 cm), (ii) a 2D lab-scale setup (60 cm × 30 cm) and (iii) a 2D field-scale domain (20 m × 4 m). In these setups, synthetic dissolved oxygen data and forward reactive transport simulations are used to image the spatial distribution of As-bearing pyrite using the Principal Component Geostatistical Approach (PCGA) for inverse modeling.

1. Introduction

Accurate identification of physical and geochemical aquifer properties controlling groundwater contaminant behavior is critical for reliable contaminant plume prediction, remediation design and operation, and effective management of groundwater resources. Spatially distributed physical and geochemical heterogeneities control solute transport in groundwater; thus, they are of pivotal importance for understanding the fate of contaminants in the subsurface. Over the last few decades, numerous studies have focused on identifying spatially distributed physical properties of aquifers including hydraulic conductivity, porosity, and specific storage. Examples of widely used characterization techniques include pressure-based methods, such as hydraulic tomography [1–4], and geophysical-based methods including electrical resistivity tomography [5,6] and ground penetrating radar [7,8]. The pressure-based methods use pressure measurements, which are directly sensitive and mechanistically linked to the physical parameters of interest through the groundwater flow equation, to infer the spatial parameters, i.e., hydraulic conductivity fields. The geophysical-based methods can be used to map lithologic heterogeneities in regions that are difficult to install bore wells and implemented jointly with pressure-based methods. These techniques have been applied to successfully estimate or "image" the physical heterogeneity of the subsurface in field cases (e.g., [1]). Here, and throughout this manuscript, the term “imaging” is used to describe the estimation of the spatial distribution of an aquifer property of interest.

The spatial distribution of biogeochemical properties exerts a key control on contaminant transport. For instance, the heterogeneous distribution of organic matter in aquifer systems is necessary for understanding the sorption of both organic compounds

47 [9–12] and inorganic contaminants, including arsenic [13–19]. Similarly, the location of
48 reactive mineral phases can control the fate of metals and metalloids [20–22], mineral
49 precipitation/dissolution rates [23], and bioclogging [24] in porous media. Therefore, to
50 quantitatively understand contaminant transport and to implement successful
51 groundwater management strategies, it is important to characterize the spatial distribution
52 of geochemical properties. However, only a limited number of studies have been
53 conducted to infer spatially heterogeneous geochemical fields, likely due to (1) the
54 limited amount of sparse measurements available at the field scale, (2) the challenge in
55 formulating quantitative descriptions of controlling geochemical processes in the
56 framework of groundwater flow and reactive transport models, and (3) the complexity
57 and computational burden associated with multi-species reactive transport modeling-
58 based inversions. Recent works overcome the former by applying geophysical-based
59 methods to estimate the spatial distribution of reactive elements and mineral phases [25–
60 31] as well as reactive facies [32,33]. While these methods have been successfully
61 applied to field settings with promising results, these approaches still require collecting a
62 large amount of geochemical data to develop a site-specific petrophysical relationship
63 (from geophysical to hydro-geochemical properties) or correlation while the true
64 relationship may not be unique or one-to-one [34]. In this study, we propose an effective
65 geochemical imaging method using reactive transport based inverse modeling as well as
66 the information content of sparse groundwater chemistry data perturbed by the
67 controlling geochemical processes. We demonstrate the capability of the proposed
68 method to image spatially distributed geochemical properties of several synthetic
69 domains using sparse aqueous concentration data. We focus on geochemical

environments relevant to the mobilization of arsenic via mineral dissolution in aquifer systems. In the last few decades, numerous studies have focused on understanding geochemical controls of As mobilization. While these studies have greatly contributed to developing a geochemical framework for As reactivity in the environment, arsenic contamination of groundwater remains problematic in aquifers throughout the world. Research efforts can be enhanced by developing inexpensive and efficient methods for quantifying As distribution in aquifer sediments.

Arsenic is a toxic metalloid and a naturally occurring contaminant that poses a significant threat to groundwater quality. The release of native As from sediments into surrounding pore water can be attributed to shifts in water chemistry via four principal mechanisms: (1) ion-displacement (2) shifts in pH to alkaline values exceeding 8.5 (3) reduction of arsenate to the more labile arsenite and (4) dissolution of arsenic-bearing minerals [35–37]. The spatial distribution of As-bearing heterogeneities is a controlling factor in all the above-mentioned processes. Here, we focus on a mechanism (4) which is relevant in natural and managed aquifers with fluctuating redox environments [38–46]. Specifically, we are interested in imaging As-bearing sulfidic minerals such as arsenopyrite and arsenian pyrite which can be a source of dissolved As in groundwater, particularly in shifting redox environments including injection of oxidizing recharge water into previously anoxic aquifers as part of aquifer storage and recovery operations [47–50].

The outline of the paper is as follows: in Section 2, we present the proposed methodology for forward and inverse modeling. The forward reactive transport model describes the mobilization of As via kinetic oxidative dissolution of As-bearing pyrite

due to dissolved oxygen (DO) in the ambient groundwater. The inverse model is based on the computationally-efficient Principal Component Geostatistical Approach (PCGA) [3,51]. Considering increasing complexity and accounting for the scale-dependent spatial distribution of As-bearing minerals (Figure 1), the modeling investigation was carried out at multiple scales and considered different flow-through domains including (i) a 1D lab-scale column (80 cm), (ii) a 2D lab-scale setup (60 cm × 30 cm) and (iii) a 2D field-scale cross section (20 m × 4 m). In Section 3, we illustrate the results obtained using DO observations at selected locations, and forward and inverse modeling to produce the best estimate of the spatial distribution of As-bearing pyrite. We also analyzed the estimation uncertainty and performance of the PCGA-based inverse method. Concluding remarks are provided in Section 4.

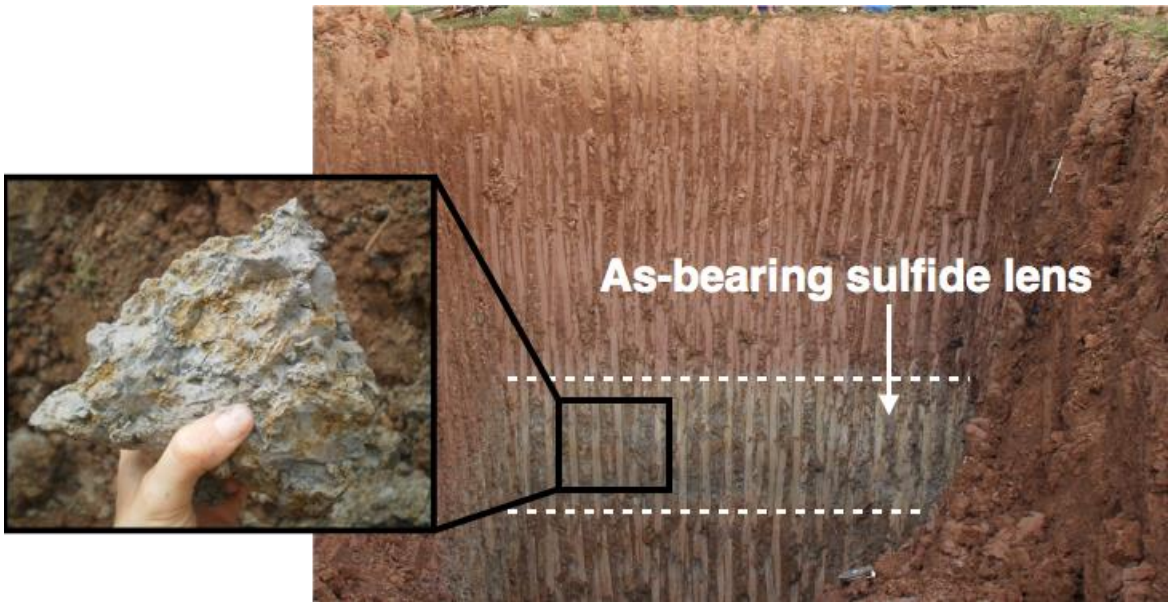

Figure 1: Spatial distribution of arsenic-bearing sulfidic minerals (grey in color) at a 6 m depth (right) in sediments of the upper Mekong Delta, Cambodia. The distribution of sulfidic minerals has scale-dependencies as seen by the centimeter-variation within the sediments (left).

2. Methods

The Principal Component Geostatistical Approach (PCGA) is a fast Jacobian-free geostatistical inversion approach that uses the leading principal components of the prior information to save computational costs. In this study, we propose the application of this method with reactive transport simulations of arsenic release. We used a forward reactive transport model including equilibrium and kinetically-controlled reactions and applied the methodology to 1-D bench-, 2-D bench-, and 2-D field-scales to estimate underlying As-bearing pyrite distributions and the corresponding estimation uncertainties. The method was implemented in MATLAB using MODFLOW [52] and PHT3D [53] to develop the flow and reactive transport forward model. In the following subsections, we describe the forward model, the PCGA inversion method, and the model parameters and domain properties of the various domains analyzed.

2.1 Forward model

The forward reactive transport model includes a reactive network developed with the geochemical code PHREEQC [54] and coupled to groundwater flow and multicomponent transport using PHT3D [53]. PHT3D uses a finite difference approximation to solve numerically the governing mass conservation equations, which for reactive solute transport of mobile aqueous components and immobile entities (e.g., minerals) read as:

$$\frac{\partial C_n}{\partial t} = \frac{\partial}{\partial x_\alpha}\left(D_{\alpha\beta}\frac{\partial C_n}{\partial x_\beta}\right) - \frac{\partial}{\partial x_\alpha}(v_\alpha C_n) + \frac{q_s C_n^s}{\theta} + r_{reac,n}$$
$$\frac{\partial C_n}{\partial t} = r_{reac,n} \quad (1)$$

where C_n is the total aqueous component concentration of the n^{th} component [53], v_α is the seepage velocity in direction x_α, $D_{\alpha\beta}$ is the hydrodynamic dispersion coefficient tensor, q_s is a volumetric flow rate representing sources and sinks, θ is porosity, is the concentration of the source or sink, and r_{reac} is a term describing the source/sink chemical reaction rate.

2.1.1 Physical properties

The influence of heterogeneity of physical properties for transport in porous media has been investigated in a number of contributions from pore to field scales (e.g., [55–59]). In order to focus on the estimation of chemical heterogeneities, the modeled domains were assumed to be physically homogenous with a uniform flow regime. The physical model properties are included in Table 1.

Table 1: Geometry of the domain and parameters for the forward reactive transport model

Parameter	**Model Domain**		
Physical properties	**1D bench**	**2D bench**	**2D field**
Width (m)	0.8	0.6	20
Height (m)	0.01	0.3	4
Rows	1	30	50
Columns	80	60	100
Grid size in x and y (Δx, Δy)	0.01	0.01/0.01	0.4/0.08
Porosity	0.4	0.4	0.4
Hydraulic Conductivity (m/day)	17.5	17.5	35.5
Molecular diffusion coefficient (m^2/day)	3.5×10^{-5}	3.5×10^{-5}	3.5×10^{-5}
Longitudinal dispersivity [a] (m)	7.7×10^{-4}	7.7×10^{-4}	2.0×10^{-2}
Transverse dispersivity [a] (m)	-	7.7×10^{-5}	2.0×10^{-3}
Seepage velocity (m/day)	0.5	0.5	3.7
Solid-phase components			

Concentration pyrite [b] (mg/kg soil)	7498.8	7498.8	2249.6
Concentration As (mg/kg soil)	70.3	70.3	21.1
As in pyrite (wt %)	0.94%	0.94%	0.94%

Influent aqueous concentrations (mol L^{-1})

pH	HCO_3^-	Cl^-	Fe_T	Na^+	DO	SO_4^{2-}	As_T
7	1.0×10^{-3}	1.0×10^{-3}	0	1.82×10^{-3}	2.75×10^{-3}	1.0×10^{-6}	0

[a] values consistent with those reported in high-resolution laboratory [60] and field investigations [61,62]

[b] values within range of concentrations listed in [63]

142

143 *2.1.2 Chemical reaction framework*

144 The forward simulations were based on a reaction network including 57 aqueous
145 equilibrium speciation half reactions, 2 kinetic mineral reactions, 13 surface
146 complexation reactions and reproduced scenarios in which an initially anoxic solution is
147 displaced by an aerated solution of the same ionic composition containing 2.75×10^{-4}
148 mol/L of dissolved oxygen. We focus on the redox reaction resulting in the oxidative
149 dissolution of As-bearing pyrite due to the introduction of oxygenated water. The
150 chemical composition of the influent solution (Table 1) is identical to the initial solution
151 except the initial solution is anoxic and does not contain oxidized species. The reaction
152 network is similar to networks used in previous studies of arsenic reactive transport (e.g.
153 [64,65]) The introduction of oxygen into the previously anoxic domain results in the
154 kinetic oxidative dissolution of As-bearing pyrite. Briefly, the rate of pyrite oxidation was
155 defined by the following expression developed by [66] and previously used in field
156 applications [48,67]:

$$r_{pyr} = {C_{O2}}^{0.5} {C_{H+}}^{-0.11} \left(10^{-10.19} \frac{A_{pyr}}{V}\right) \left(\frac{C}{C_0}\right)_{pyr}^{0.67} \quad (2)$$

157 where r_{pyr} is the rate of pyrite oxidation (mol/L/s), and C_{O_2} and C_{H^+} are the aqueous
158 concentrations of oxygen and hydrogen ions, respectively (mol/L). A_{pyr}/V is the ratio of

pyrite surface area to the volume of solution and is set to 115 [48]. C/C_0 is a factor accounting for surface area changes resulting from the dissolution of pyrite. While reaction (1) is slightly pH dependent, the bicarbonate in the groundwater buffers the solution pH. The release of As(III) was simulated as stoichiometrically linked to the oxidation of pyrite [50,64,65] which follows the following reaction:

$$FeS_2 + 3.75O_2 + 0.5H_2O \rightarrow Fe^{3+} + 2SO_4{}^{2-} + H^+ \quad (3)$$

The molar fraction of As to pyrite was set to 0.015 and was within previously reported ranges of sedimentary materials [63,68].

During the modeled dissolution of As-bearing pyrite, dissolved As(III) was oxidized to As(V) which was the dominant As specie at steady-state. Additionally, ferrous iron was released and subsequently oxidized to ferric iron. This resulted in the precipitation of ferrihydrite (HFO) which can sorb As and retard the transport of this contaminant. The rate of HFO formation is kinetic and was expressed as

$$r_{HFO} = k\left(1 - \frac{IAP}{K_{SP}}\right) \quad (3)$$

where r_{HFO} is the rate of formation of HFO, k is an empirically derived constant set to 10^{-14} mol m^{-2} s^{-1} [65], and IAP/K_{sp} is the saturation ratio of ferrihydrite. The surface complexation of As(III) and As(V) species on ferrihydrite was modeled as an equilibrium-controlled process with a sorption site density of 0.2 mol/mol ferrihydrite and a surface area of 600 m^2/g [69].

While other geochemical processes such as ligand exchange, competitive sorption can affect arsenic transport (e.g., [16,70–72]), we focused on the oxidative dissolution of reduced minerals as the main controlling mechanisms. We assumed DO concentrations

were controlled by the consumption of oxygen during the oxidation of sulfidic minerals. Accordingly, we used distributed observations of DO to image the heterogeneous distribution of As-bearing pyrite inclusions. In natural settings, DO consumption will be a result of numerous geochemical processes inclusive of the oxidation of organic matter and formation of oxide minerals such as manganese oxides which are both processes that can affect the cycling of As in sediments (e.g., [18,73–75]). However, field-scale studies have successfully simulated DO measurements by focusing on oxidative dissolution of sulfidic minerals as the controlling process [64]. Therefore, we focus only on the oxidative dissolution of As-bearing sulfides and precipitation of Fe (hydr)oxides as DO consuming processes. Other processes can be accounted for with the error added to simulated DO measurements as described below.

2.2 Inverse model

We used the PCGA to determine the spatial distribution of As-bearing pyrite from a limited number of observations of DO concentrations while other parameters in Equations (1) and (3) were assumed to be known and are provided in text. The PCGA is a fast large-scale and joint inversion approach based on the geostatistical inverse method [76,77], which is widely used for spatially distributed subsurface property calibration problems. Here, we include a brief description of the geostatistical method followed by a description of the PCGA.

2.2.1 Overview of the geostatistical approach

The objective of the geostatistical approach is to determine a vector of unknowns from a vector of observations in a Bayesian framework. The observation equation is given by:

$$\boldsymbol{y} = h(\boldsymbol{s}) + \boldsymbol{v} \quad (4)$$

where **y** is the vector of observations, *h* is the forward model, **s** is the unknown variable, and **v** is a Gaussian term accounting for error in the observations and forward model. The prior probability of **s** is assumed to be Gaussian with an unknown mean and a prior covariance matrix **Q**. Using this assumption, the posterior pdf of **s** is calculated using Bayes' theorem and the negative log likelihood of the posterior pdf forms the objective function. By minimizing the objective function, the maximum a posteriori (MAP) estimate or most likely value of **s** is obtained. This minimization of the objective function is a nonlinear optimization problem that is commonly solved using iterative Gauss-Newton method where the initial guess is repeatedly updated to obtain a new As-bearing pyrite distribution fitting the data. Specifically, in this application focused on imaging reactive As-bearing minerals, **y** is the oxygen concentration at monitoring well, *h* is reactive transport model, and **s** is spatially distributed As-bearing pyrite concentration.

While the geostatistical method is well suited for small- to moderate-scale inverse problems, it becomes computationally challenging and costly for large-scale inversions. Furthermore, the geostatistical method requires computation of the derivative of the forward problem (Jacobian matrix, i.e., sensitivity of the observations to the unknowns) which typically requires intrusive changes in the forward model code which is challenging for multi-physics problems that utilize coupled forward models.

2.2.2 The principal component geostatistical approach

The PCGA expedites the geostatistical inversion by avoiding the direct evaluation of the Jacobian. As a result, the number of numerical simulations can be reduced by a factor of 10 or more with controlled accuracy in most cases. The PCGA avoids the direct

computation of the Jacobian by utilizing a low-rank approximation of the covariance **Q** and a finite difference approximation of all matrix-vector products. **Q** is approximated through:

$$\mathbf{Q} \approx \mathbf{Q_K} \approx \boldsymbol{ZZ^T} \approx \sum_{k=1}^{K} \zeta_i \zeta_i^T \tag{5}$$

where $\mathbf{Q_K}$ is a rank-*K* approximation of **Q**, **Z** is a *m* by *K* matrix and ζ_i is the *i*-th column vector of **Z**. A fast method to obtain Equation (5) for large-scale covariance matrices is explained in [3]. Approximately "*K*" forward simulation evaluations are needed to obtain the inverse solution. By applying Equation (5), the PCGA can reduce the number of numerical forward simulations greatly, usually up to a few hundred simulation runs, which is highly beneficial for complex multi-species reactive transport problems, while inverse solutions are almost the same as those obtained from the conventional geostatistical approach as shown in [3].

To enforce positivity in the estimation of As-bearing pyrite concentrations (C_{pyr}) we used a square-root transformation:

$$\mathbf{s} = \sqrt{\boldsymbol{C_{pyr}}} \tag{6}$$

This transformation can be seen as a simplified version of Box transformation [78], which has been used to contaminant source identification applications (e.g., [79,80]). The prior pdf of **s** was assumed to be Gaussian with unknown mean and exponential covariance, **Q**. Numerical simulations and inversion were carried out on a Linux workstation equipped with Intel 16 core 3.1 GHz processors and 128 GB RAM.

2.3 Problem setup

2.3.1 1-D bench

Beginning with a simplified domain, we simulated the oxidation of As-bearing pyrite from a 1-D laboratory column of approximately 80 cm in length. The column contained a 30 cm long inclusion of As-bearing pyrite in an otherwise homogenous domain as shown in Figure 2b. The spatial and temporal changes in chemistry during the forward reactive transport simulation are illustrated in Figure 2 for this 1-D domain. As a result of oxidative dissolution, dissolved As, Fe(III) and SO_4^{2-} were released from the pyritic mineral lens (Figure 2a). Ferric iron was released at a lower concentration than SO_4^{2-} due to the precipitation of ferrihydrite (Figure 2b) and the lower abundance of Fe than S in the pyritic minerals. The transport of As is also affected by the adsorption on ferrihydrite surfaces. The 1-D column simulation reached pseudo-steady state conditions after approximately 1.5-day simulation time (Figure 2c) in which the outlet concentrations of dissolved chemical species were stable due to the slow dissolution of As-bearing pyrite. After sufficient time, all the As-bearing pyrite will react and leave the system, but due to the slow kinetics of As-bearing pyrite dissolution the system reaches a pseudo-steady state in which the reaction byproduct concentrations are unchanged. Among the dissolved chemical species, we assumed that the steady-state oxygen concentrations were collected as the observation data for the inversion. This water chemistry parameter was selected due to its key importance for oxidative dissolution of reduced minerals and since currently available oxygen measurement sensors are relatively inexpensive, accurate and operable in real-time. Such sensors have been recently used to obtain high-resolution distributed measurements of oxygen in laboratory setups [81–84] and field applications [85]. Gaussian random noise with a standard deviation of 2% of the maximum oxygen consumption (10^{-6} mol/L) was added to the

observations to represent measurement and conceptual modeling errors in a well-controlled column experiment. The number of observations, unknowns and magnitude of measurement error are listed in Table 2.

Table 2: Parameters of the inverse model carried out using the PCGA approach

Parameter	**Model Domain**		
	1D bench	**2D bench**	**2D field**
Number of observations	5	20, 50, 75, 150	250
Number of unknowns	80	1800	5000
Number of principal components, *K*	80	32, 64, 96, 192	96
Covariance kernel, *q*	exponential	exponential	exponential
Correlation length λ (m)	0.6	$\lambda_x = 0.6$, $\lambda_z = 0.3$	$\lambda_x = 20$, $\lambda_z = 4$
Variance	0.1	0.1	0.1
Measurement error (mol/L)	10^{-6}	10^{-6}	2.5×10^{-5}, 5×10^{-5}

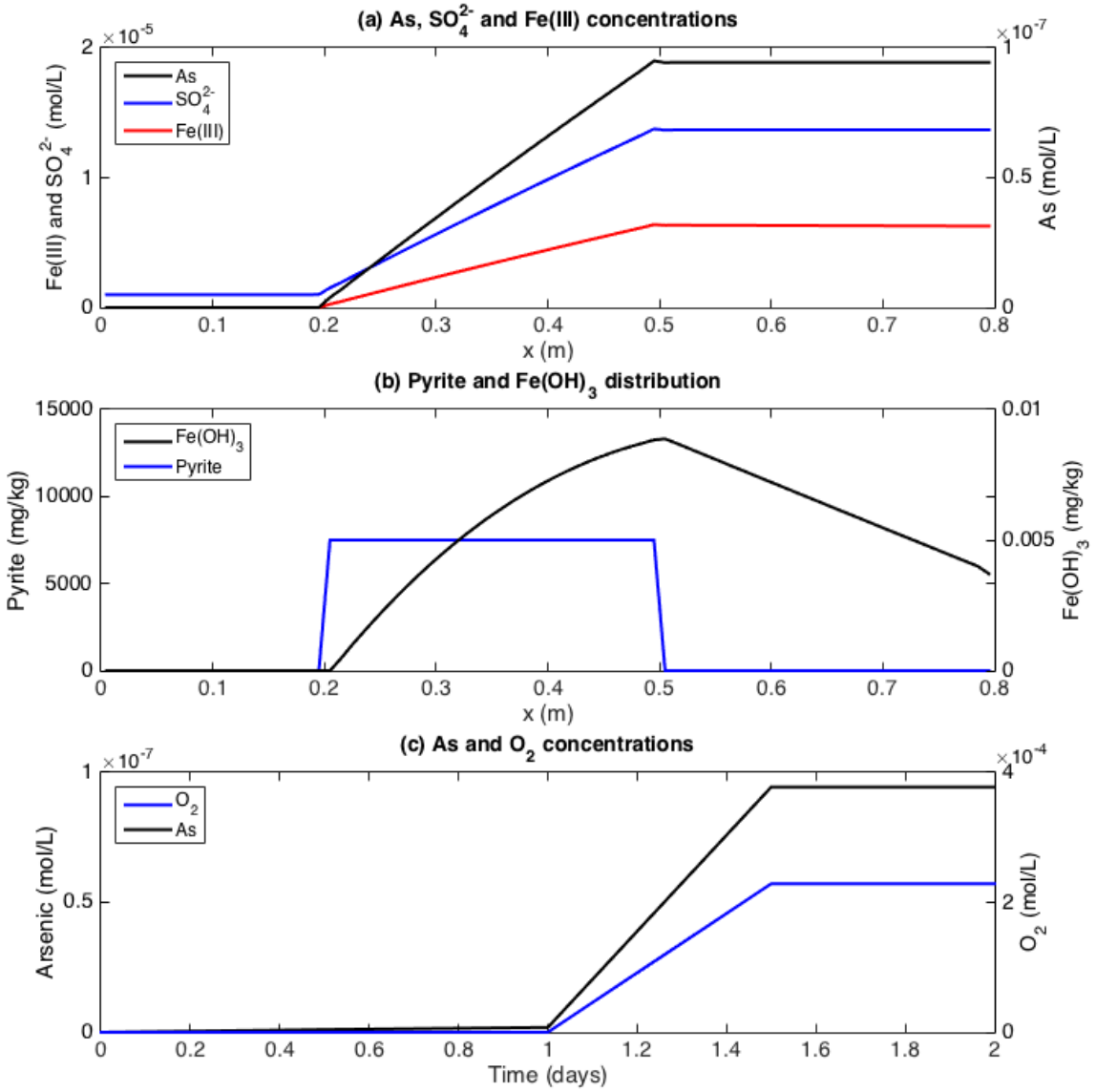

Figure 2: (a) Spatial profiles of dissolved As, SO_4^{2-} and Fe(III) concentrations at pseudo-steady state (2 days). (b) Solid-phase concentrations of pyrite at pseudo-steady state which diminished from initial concentration of 0.3 mol/L and Fe (hydr)oxides which form as a result of pyrite oxidative dissolution and subsequent oxidation of Fe(II). (c) Breakthrough curves of As and O_2 concentrations (mol/L) at the outlet of the domain.

2.3.2 2-D bench scale

Next, we imaged As-bearing pyrite inclusions in a 2-D bench-scale system. The 60 by 30 cm domain contained two 11 by 7 cm box-shaped inclusions in an otherwise homogenous system as shown in Figure 4a. We assumed that five vertical arrays of oxygen sensors were installed every 15 cm (x = 0, 0.15, 0.3, 0.45 and 0.6 m) (Figure 4a). A measurement error of 4% of the maximum oxygen consumption was added to the observed concentrations simulated from "true" As-bearing inclusions. Using this domain, we examined (1) the number of forward simulation model runs, i.e., the number of principal components (K) needed to obtain a reliable estimate of the unknown field and (2) the effect of the number of measurements on the accuracy of the best estimate.

2.3.3 2-D field scale

To demonstrate the potential of the proposed approach to map complex patterns of field-scale geochemical heterogeneities, we expanded our analysis to a 20 m × 4 m cross-sectional domain. For this scenario, the spatial distribution pattern of geochemical heterogeneity was generated stochastically: two realizations of Gaussian random fields from an anisotropic exponential covariance model [86] were thresholded to obtain two random binary As-bearing pyrite distributions as shown in Figure 7a.

3. Results and Discussion

3.1 1-D bench scale

The "true" field shown in Figure 3a was used to generate five steady-state synthetic concentration measurements with observation locations displayed as red circles in Figure 3c. Because this 1-D forward problem can be solved efficiently in 5 seconds, the PCGA with all K = 80 principal components (i.e., equal to the number of grid cells)

was used to estimate the underlying As-bearing pyrite concentrations to illustrate how the inversion approach performs for geochemical heterogeneity identification. In this case, low-rank approximation was not used and the approximation error only comes from the finite difference approximation in the inverse method. Inversion with smaller number of principal components is presented in the 2-D simulations. While the initial guess was set to a homogeneous As-bearing pyrite distribution with a concentration of 5000 mg/kg across the entire domain, several initial guesses were tested and the inversion converged to the same estimate for any reasonable choice of an initial guess.

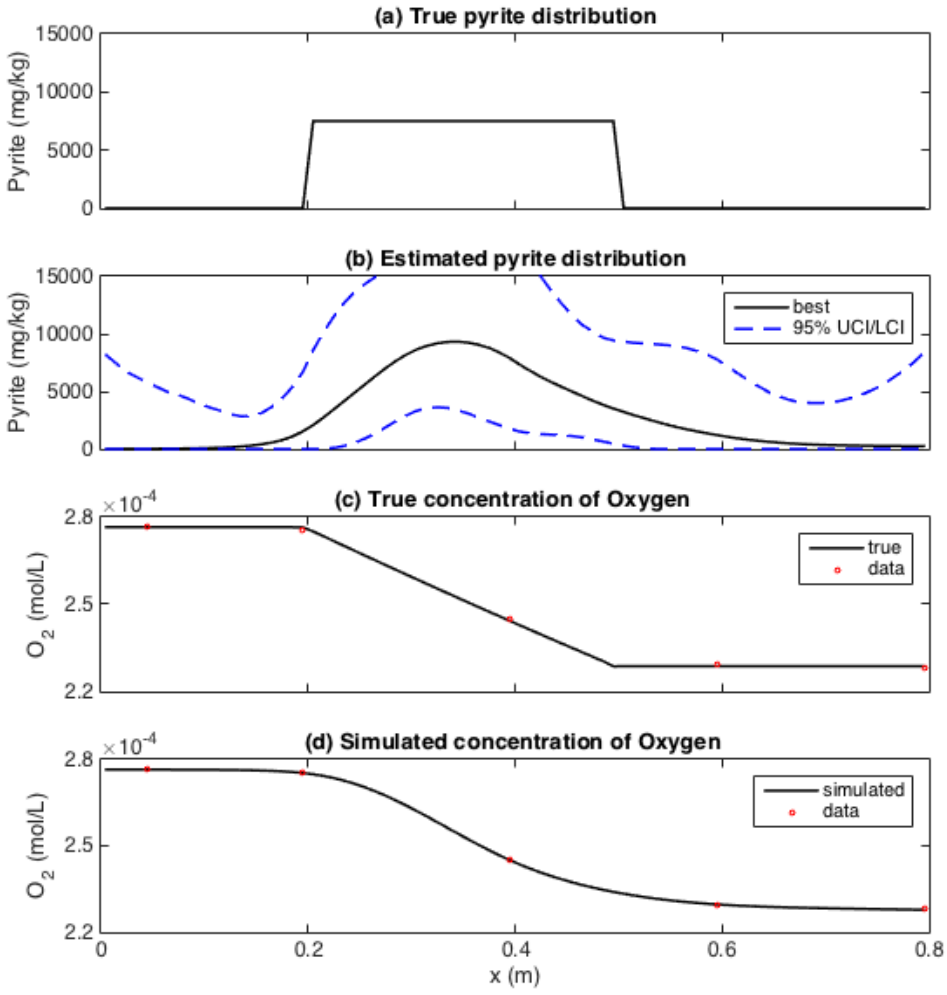

Figure 3: (a) True concentration (mg/kg) of As-bearing pyrite, (b) estimated concentration (mg/kg), (c) steady-state oxygen concentration resulting from the

oxidative dissolution of true As-bearing pyrite and selected measurements (red circles) with noise for the inversion and (d) simulated steady-state oxygen concentrations resulting from the estimated As-bearing pyrite and reproduced oxygen concentrations (red circles) at the monitoring locations

A total of 329 forward model runs (converged with 4 iterations) were used to obtain the result on 16 processors in 5 minutes. Structural parameters such as noise level, prior variance and correlation length were chosen using Q2/Cr criteria [87] which provides a framework for selecting the model parameters to be used for the inversion. The resulting parameter values are reported in Table 2. The inversion successfully captures the location and magnitude of the true As-bearing pyrite concentration (Figure 3b) while the estimated distribution is smooth due to the Gaussian distribution assumption of the prior. The true As-bearing pyrite distribution is located within the 95% confidence interval (Figure 3b) of the inversion. Confidence interval was relatively wide at the constant concentration boundary condition (x = 0 cm) and the most downstream (x = 80 cm). Because of the fixed boundary condition at x = 0 cm and advective information propagation, the information of measurements at both locations is almost zero, resulting in the high uncertainty around the both ends. The estimated pyrite reproduces the DO measurements accurately within measurement error as shown in Figure 3d. This simple experiment demonstrates that a reasonable estimate can be achieved with a few hundred simulation runs even with only a few sparse oxygen measurements.

3.2 2-D bench scale

The true field for a 2-D bench-scale domain (Figure 4a) was used to generate the DO observation measurements in Figure 4a. These measurements were successively used for the PCGA-based inversion to image the location and the concentration of the As-bearing reactive mineral inclusions in the 2-D domain.

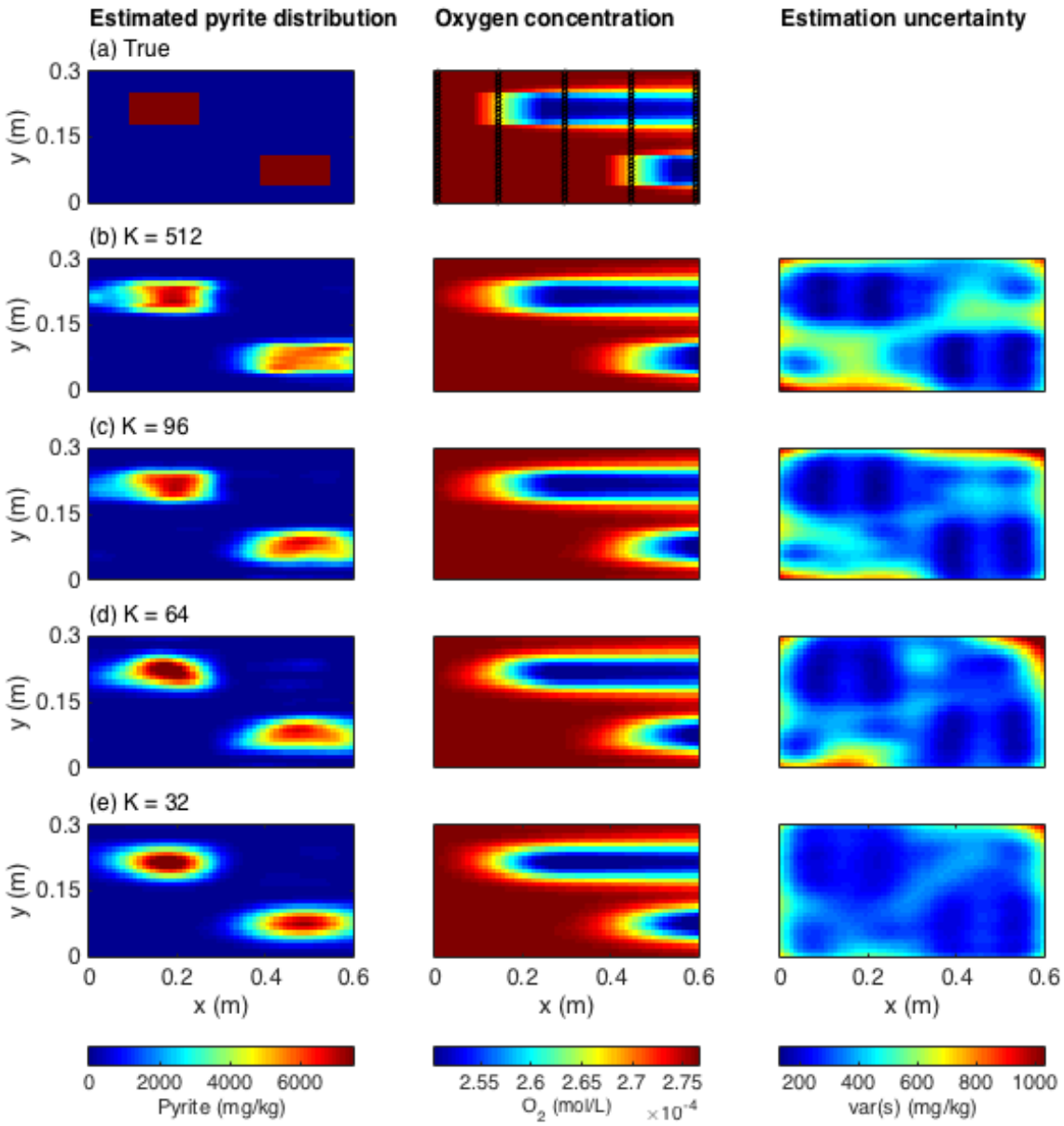

Figure 4: The effect of the number of principal components (K) on the pyrite distribution estimate. (a) shows the true pyrite distribution (first column) and

corresponding oxygen concentration (second column) along with the DO measurements which are highlighted with black markers. The best estimates of pyrite distribution, corresponding simulated oxygen concentration and variance of estimate are shown for K = (b) 512, (c) 96, (d) 64, and (e) 32.

3.2.1 Effect of number of principal components (K)

Initially, it was assumed that each sensor array collected a DO depth profile with measurements every 1 cm in depth, which amounts to a total of 150 measurements used in the inversion. To investigate an optimal number of principal components in this application, K = 512, 96, 64 and 32 principal components were used to estimate the underlying pyrite concentration. Sixteen multiples of K values were assigned to take advantage of parallel executions on the 16-core workstation. For K = 512, a total of 2576 forward simulations were executed to find a best estimate in around 10 hours; while for K = 32, total 176 simulations were run in 40 minutes.

The best estimates are presented in Figure 4b-4e. Even with only 32 principal components, the inversion was able to capture the location and magnitude of the underlying pyrite lenses. Also the best estimate of the oxygen consumption, obtained with the different numbers of principal components, closely reproduced the pattern observed in the true field. We used the root mean square error (RMSE) as a quantitative metric to assess the performance of the inversion. Calculating the RMSE of the best estimate as compared to the true distribution, we observed that it does not change significantly as a function of K (Figure 6a). This is due to the simple geometry of the true

concentration field, which only requires a relatively small number of simulations to obtain a reasonable estimate.

While the estimated location of the pyrite lenses can be accurately determined with a small number of principal components, the estimation uncertainty was generally underestimated because of the approximation used in Equation (4). Increasing K resulted in decreased RMSE of the uncertainty as shown in Figure 6c. Thus, it is recommended that more principal components be added to accurately quantify estimation uncertainty. While this requires more simulation runs, starting with a moderate number of K values and increase K when convergence is achieved, the correct estimation uncertainty can be gained.

3.2.2 Effect of number of measurement points

To evaluate the efficiency of the inversion approach, the effect of the number of data measurements used in the inversion was examined. Figures 5b-5e show the best estimates for the location and concentration of the As-bearing pyrite inclusions, the corresponding oxygen consumption and the computed estimation uncertainty with 150, 75, 50, 20 measurements which corresponds to 1, 2, 3 and 7.5 cm vertical spacing of measurement locations, respectively. Good estimates of As-bearing pyrite distribution were obtained for the cases considering at least 50 data points. The quality of the image deteriorates significantly for the case using only 20 measurement points. Inversion with 20 measurements (7.5-cm spacing which is larger than the 7-cm height of the pyrite lens) resulted in poor identification of the pyrite distribution. In this case, the method did not capture the bottom-right inclusion and also the concentration range of the image becomes rather dissimilar from the true field. This results from the impossibility of the very sparse

observation network to capture the oxygen concentration gradients due to oxidative dissolution in the lower part of the domain. Again, we used RMSE to quantitatively evaluate the performance of the inversion as a function of the number of observation points. We observed that the RMSE decreases significantly with increasing number of observations (Figure 6b). However, it should be noted that such RMSE decrease tends to be less pronounced with larger number of measurements for the distribution of measurements examined in this domain. The results emphasize that even with a relatively small number of observations (~50 measurement points), the proposed approach was able to identify the location and magnitude of the As-bearing pyrite distribution while smaller number of data measurements could result in errors in the estimation of the sulfidic mineral location.

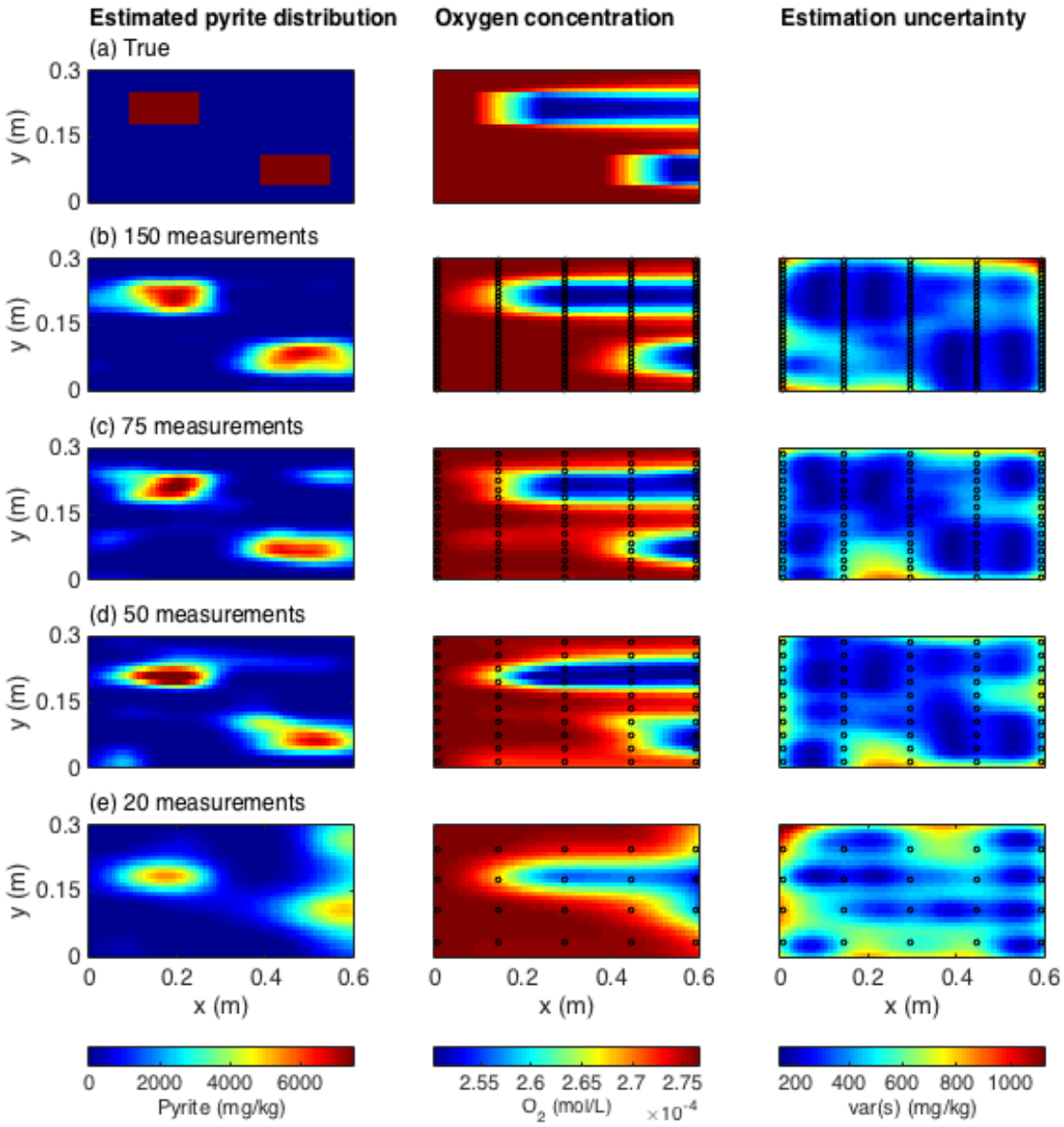

400

401 **Figure 5: Effect of the number of measurements on pyrite estimates. The true pyrite**
402 **and oxygen distributions are shown in (a). The best estimates of pyrite distribution,**
403 **corresponding simulated oxygen concentration and uncertainty are shown for (b)**
404 **150, (c) 75, (d) 50, and (e) 20 total measurements. Black circles highlight the location**
405 **of the dissolved oxygen measurements.**

406

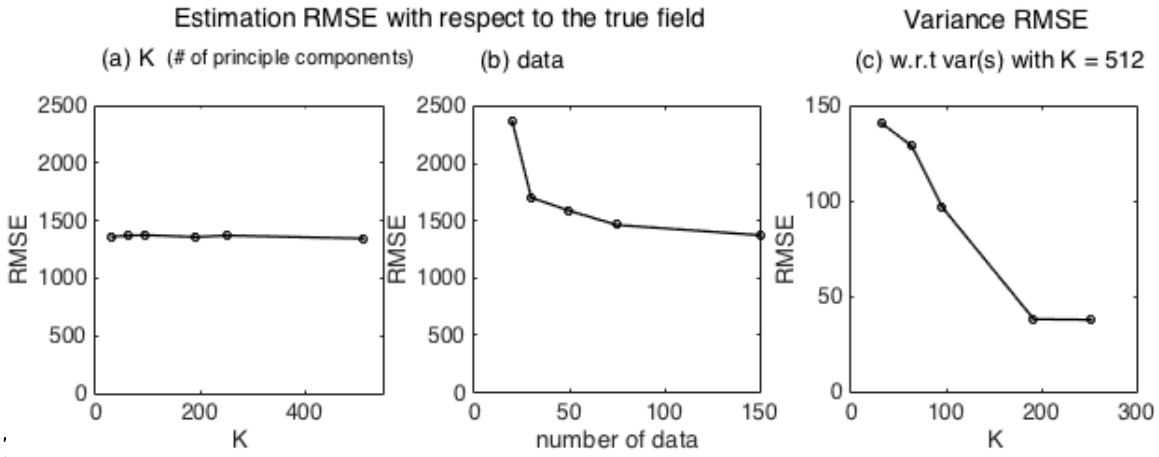

40'

408 **Figure 6: RMSE as a function of (a) the number of principal components, (b)**
409 **number of measurement points used in the inversion and (c) RMSE relative to**
410 **uncertainty of the best estimate for 512 principal components.**

411 **3.3 2-D field scale**

412 Lastly, field-scale characterizations were performed to study potential
413 applications of the inversion method. Two random heterogeneous fields were generated
414 and tested as shown in Figures 7a and 7b. Oxygen sensor arrays are assumed to be
415 located at x = 0, 4, 8, 12, 16 and 20 m and at each array, sensors were installed every 0.25
416 m corresponding to a total of 96 measurement points for this analysis. Larger error of 10%
417 and 20% of the maximum oxygen consumption was added to the simulated
418 concentrations to reflect higher uncertainty at the field-scale. The best estimates are
419 shown in Figure 7. With measurement error of 10% and irregularly distributed
420 heterogeneities, the inversion method can accurately identify the location of the As-
421 bearing pyrite lenses. At 20% measurement error, difficulties were encountered in
422 capturing the location and magnitude of all the heterogeneities, particularly small pyrite

lenses. We also performed forward simulations using the best estimate of the spatial distribution of pyrite to analyze the capability of the inversion results to reproduce the arsenic plumes from the true pyrite distribution. The estimated As-bearing pyrite locations and magnitude reproduced the main features and the multiple plumes of dissolved As within the simulated aquifer (Figure 8). With 10% measurement error, the location of all high As concentration plumes were accurately captured although the magnitude was slightly underestimated. With 20% measurement error the main arsenic plumes are still correctly located but not all chemical heterogeneities causing As release were captured; thus, not all As plumes were reproduced and the magnitude of As concentration was underestimated, in particular in the upper plumes.

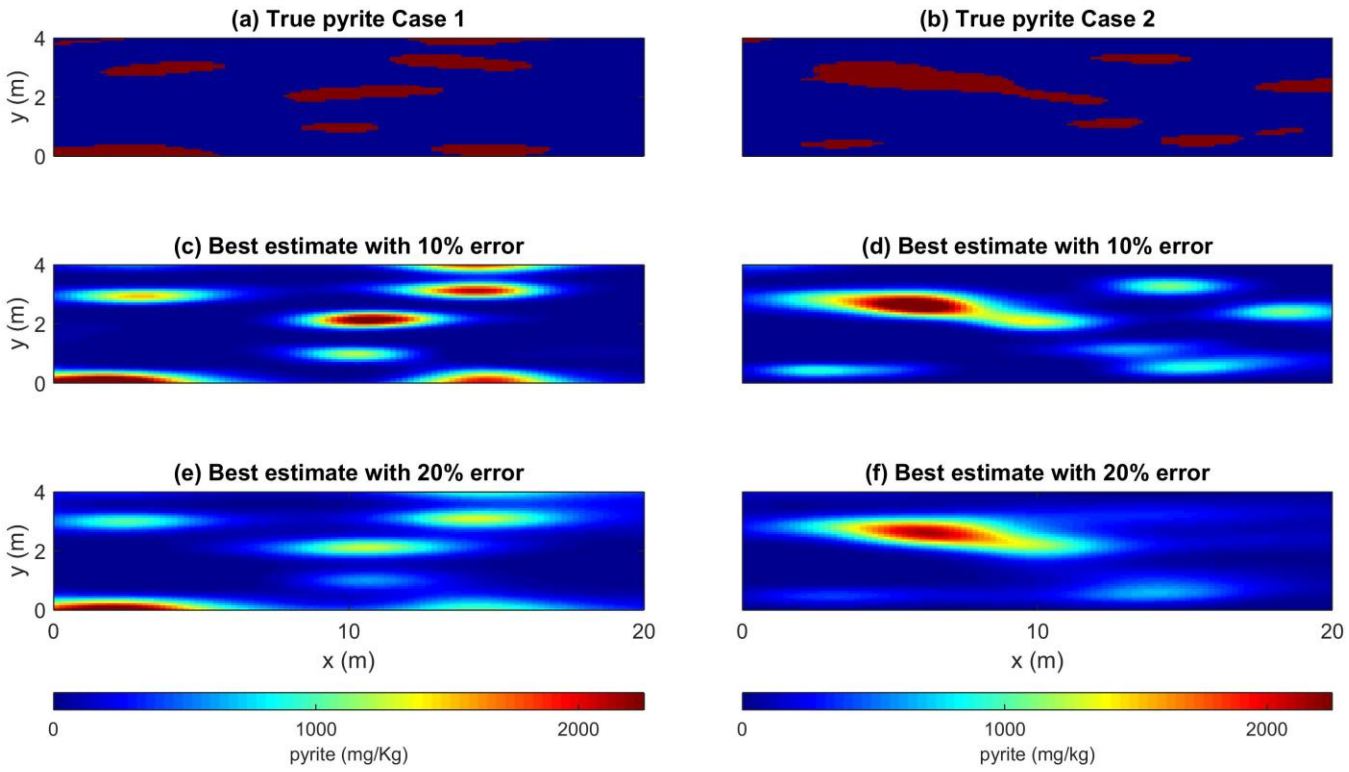

Figure 7: Best estimate maps for randomly distributed heterogeneous fields of As-bearing pyrite for (a) Case 1 with (c) 10% error, (e) 20% error, and for (b) Case 2 with (d) 10% error and (f) 20% error.

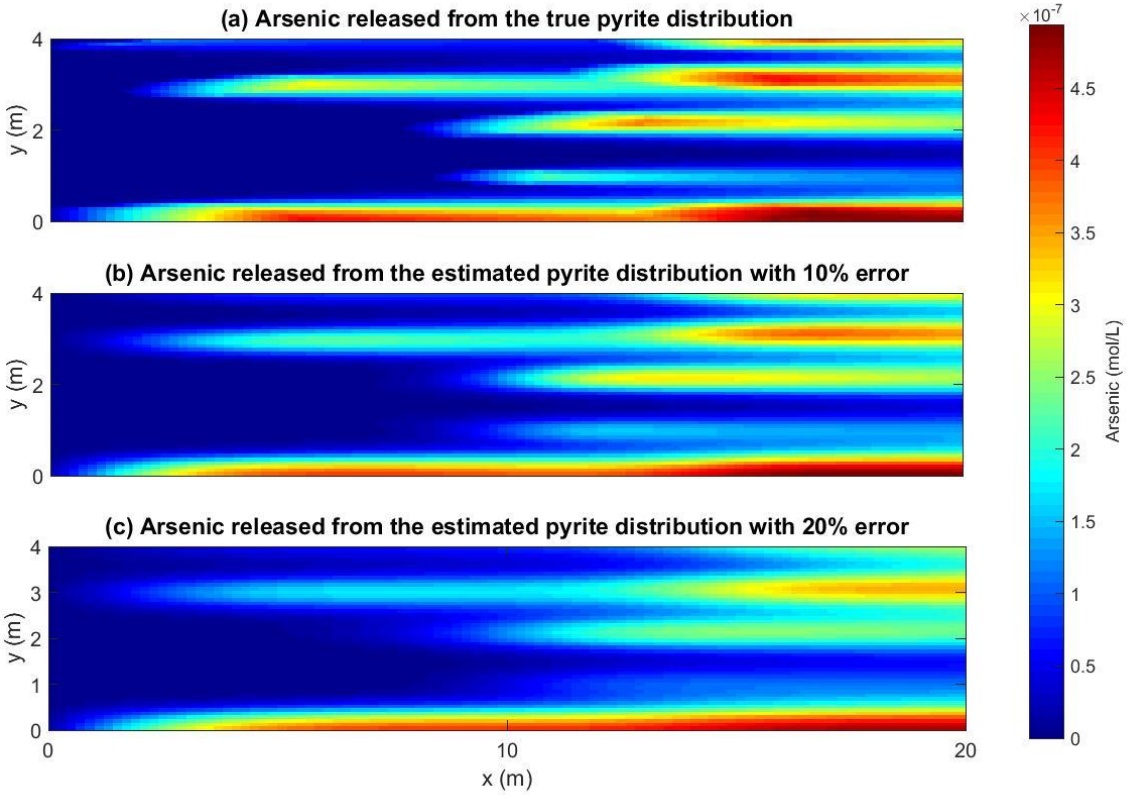

Figure 8: Dissolved arsenic concentrations at pseudo steady state for (a) the true As-bearing pyrite distribution and (b) the estimated pyrite distribution obtained in Figure 7c with 10% measurement error and (c) the estimated pyrite distribution obtained in Figure 7e with 20% measurement error.

Field-scale imaging of chemically reactive heterogeneities can be useful for a variety of applications. For example, one potential application includes managed aquifer

445 recharge (MAR) projects where shifts in native aquifer chemistry can mobilize
446 contaminants including As [48,50,63,88,89]. MAR sites in which common water quality
447 parameters are regularly monitored are potentially well-suited sites for inverse reactive
448 transport modeling methods to image reactive geochemical heterogeneities due to
449 installation of water quality monitoring well networks. Additionally, MAR sites that
450 employ aquifer storage and recovery (ASR) wells provide a unique reversal in flow
451 regime which can further enhance inversion results. Generally, upstream locations have
452 more information available through the downstream measurements. Thus, we tested a
453 scenario with reversed flow conditions, by switching downstream and upstream locations.
454 This improves the imaging results of previously down-gradient heterogeneities that
455 contained higher uncertainty. Specifically, Figure 9 shows a simulated inversion for the
456 heterogeneous field-case in which reverse flow data were used to image pyrite lenses
457 (Figure 9b) and the forward and reverse flow measurements were used in conjunction
458 (Figure 9c) to further enhance the imaging of the reactive mineral inclusions.
459 Furthermore, in the reverse flow case, previously unidentified pyrite lenses (Figure 7f)
460 are now characterized relatively well, and the combination of two different data sets with
461 higher measurement error provides a comparable result to Figure 7d, which uses
462 unidirectional flow but with smaller measurement error. RMSEs for forward flow (Figure
463 7f), reverse flow (Figure 9b) and joint (Figure 9c) cases with respect to the true field
464 (Figure 7b) are computed as 623, 585 and 557 mg/kg respectively, while RMSE of the
465 case with unidirectional forward flow and 10% measurement error (Figure 7d) is 514
466 mg/kg.

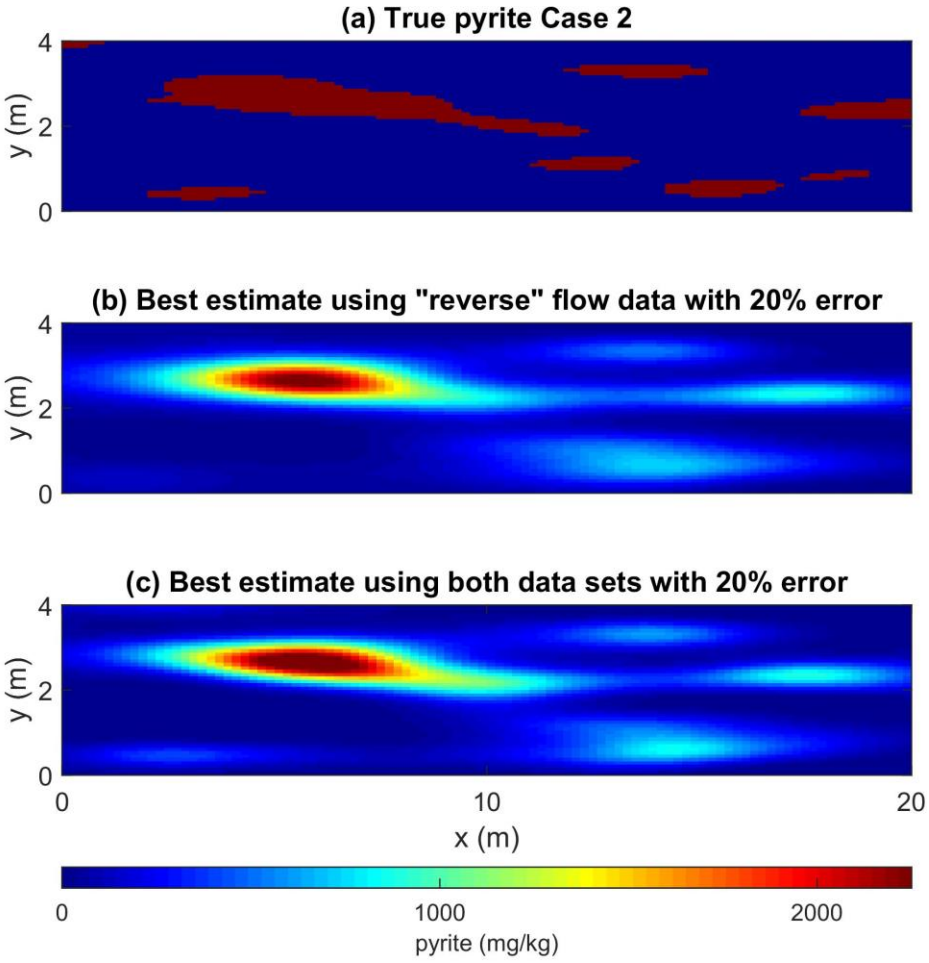

Figure 9: (a) Random, true As-bearing pyrite distribution, (b) the best estimate using only information for a reversed flow regime with 10% noise (flow right-to-left), and (c) the best estimate using data measurements from both left-to-right flow regime (Figure 7f) and the right-to-left flow regime.

4. Conclusion

Our results show that the proposed PCGA-based inverse reactive transport modeling approach can be used to image irregularly distributed As-bearing pyrite inclusions at various scales and has the potential to map complex distributions of reactive

476 subsurface properties based on the measurement of reactive dissolved constituents
477 commonly measured in groundwater. While we develop this method using a simplified
478 modeling approach, the method can be adapted to accommodate more complex reaction
479 networks. This application and similar approaches will be facilitated by rapid advances in
480 computational methods and sensor technology.

481 We demonstrated the capability and potential of inverse methods for geochemical
482 tomography by focusing on As-bearing minerals, and there are numerous additional
483 applications in which these methods can greatly help characterize subsurface
484 geochemical heterogeneities. Possible directions for exploring include: testing the
485 proposed approach with experimental observations, considering the value of information
486 of transient observations taken in different sampling events, using observations of
487 multiple parameters (e.g., dissolved oxygen with pH or other dissolved species) perturbed
488 by specific geochemical reactions.

489 Of key importance is the deployment of these methods for the simultaneous
490 characterization of both physical and chemical subsurface properties. In this study, we
491 focused on characterizing reactive chemical properties as a proof-of-concept; however,
492 coupling of physical and chemical subsurface imaging is essential for ensuring proper
493 management of groundwater aquifers and enhancing the reliability of process-based
494 reactive transport models. Additionally, the accurate determination of spatially
495 distributed physical and geochemical properties in field systems provides valuable
496 understanding of the influence of aquifer characteristics on contaminant behavior.

497

498

Acknowledgements

The research was funded by the National Science Foundation through its ReNUWIt Engineering Research Center (www.renuwit.org; NSF EEC-1028968) and a National Science Foundation Graduate Research Fellowship (NSF GRFP). M.R. acknowledges the support of the Baden-Württemberg Stiftung under the Eliteprogram for postdocs.

References

[1] Cardiff M, Barrash W, Kitanidis PK. A field proof-of-concept of aquifer imaging using 3-D transient hydraulic tomography with modular, temporarily-emplaced equipment. Water Resour Res 2012;48:W05531. doi:10.1029/2011WR011704.

[2] Cardiff M, Barrash W, Kitanidis P k., Malama B, Revil A, Straface S, et al. A Potential-Based Inversion of Unconfined Steady-State Hydraulic Tomography. Ground Water 2009;47:259–70. doi:10.1111/j.1745-6584.2008.00541.x.

[3] Lee J, Kitanidis PK. Large-scale hydraulic tomography and joint inversion of head and tracer data using the Principal Component Geostatistical Approach (PCGA). Water Resour Res 2014;50:5410–27. doi:10.1002/2014WR015483.

[4] Zhu J, Yeh T-CJ. Characterization of aquifer heterogeneity using transient hydraulic tomography. Water Resour Res 2005;41:W07028. doi:10.1029/2004WR003790.

[5] Revil A, Karaoulis M, Johnson T, Kemna A. Review: Some low-frequency electrical methods for subsurface characterization and monitoring in hydrogeology. Hydrogeol J 2012;20:617–58. doi:10.1007/s10040-011-0819-x.

[6] Slater L. Near Surface Electrical Characterization of Hydraulic Conductivity: From Petrophysical Properties to Aquifer Geometries—A Review. Surv Geophys 2007;28:169–97. doi:10.1007/s10712-007-9022-y.

[7] Davis JL, Annan AP. Ground-penetrating radar for high-resolution mapping of soil and rock stratigraphy. Geophys Prospect 1989;37:531–51.

[8] Kowalsky MB, Finsterle S, Rubin Y. Estimating flow parameter distributions using ground-penetrating radar and hydrological measurements during transient flow in the vadose zone. Adv Water Resour 2004;27:583–99. doi:10.1016/j.advwatres.2004.03.003.

[9] Allen-King RM, Kalinovich I, Dominic DF, Wang G, Polmanteer R, Divine D. Hydrophobic organic contaminant transport property heterogeneity in the Borden Aquifer. Water Resour Res 2015;51:1723–43. doi:10.1002/2014WR016161.

[10] Allen-King RM, Divine DP, Robin MJL, Alldredge JR, Gaylord DR. Spatial distributions of perchloroethylene reactive transport parameters in the Borden Aquifer. Water Resour Res 2006;42:W01413. doi:10.1029/2005WR003977.

[11] Barber II LB, Thurman EM, Runnells DD. Geochemical heterogeneity in a sand and gravel aquifer: Effect of sediment mineralogy and particle size on the sorption of

chlorobenzenes. J Contam Hydrol 1992;9:35–54. doi:10.1016/0169-7722(92)90049-K.
[12] Ritzi RW, Huang L, Ramanathan R, Allen-King RM. Horizontal spatial correlation of hydraulic and reactive transport parameters as related to hierarchical sedimentary architecture at the Borden research site. Water Resour Res 2013;49:1901–13. doi:10.1002/wrcr.20165.
[13] Redman AD, Macalady DL, Ahmann D. Natural Organic Matter Affects Arsenic Speciation and Sorption onto Hematite. Environ Sci Technol 2002;36:2889–96. doi:10.1021/es0112801.
[14] Weng L, Van Riemsdijk WH, Hiemstra T. Effects of Fulvic and Humic Acids on Arsenate Adsorption to Goethite: Experiments and Modeling. Environ Sci Technol 2009;43:7198–204. doi:10.1021/es9000196.
[15] Wang S, Mulligan CN. Effect of natural organic matter on arsenic release from soils and sediments into groundwater. Environ Geochem Health 2006;28:197–214. doi:10.1007/s10653-005-9032-y.
[16] Sharma P, Rolle M, Kocar B, Fendorf S, Kappler A. Influence of Natural Organic Matter on As Transport and Retention. Environ Sci Technol 2011;45:546–53. doi:10.1021/es1026008.
[17] Stuckey JW, Schaefer MV, Kocar BD, Dittmar J, Pacheco JL, Benner SG, et al. Peat formation concentrates arsenic within sediment deposits of the Mekong Delta. Geochim Cosmochim Acta 2015;149:190–205. doi:10.1016/j.gca.2014.10.021.
[18] McArthur JM, Banerjee DM, Hudson-Edwards KA, Mishra R, Purohit R, Ravenscroft P, et al. Natural organic matter in sedimentary basins and its relation to arsenic in anoxic ground water: the example of West Bengal and its worldwide implications. Appl Geochem 2004;19:1255–93. doi:10.1016/j.apgeochem.2004.02.001.
[19] Molinari A, Guadagnini L, Marcaccio M, Straface S, Sanchez-Vila X, Guadagnini A. Arsenic release from deep natural solid matrices under experimentally controlled redox conditions. Sci Total Environ 2013;444:231–40. doi:10.1016/j.scitotenv.2012.11.093.
[20] Englert A, Hubbard SS, Williams KH, Li L, Steefel CI. Feedbacks Between Hydrological Heterogeneity and Bioremediation Induced Biogeochemical Transformations. Environ Sci Technol 2009;43:5197–204. doi:10.1021/es803367n.
[21] Li L, Gawande N, Kowalsky MB, Steefel CI, Hubbard SS. Physicochemical Heterogeneity Controls on Uranium Bioreduction Rates at the Field Scale. Environ Sci Technol 2011;45:9959–66. doi:10.1021/es201111y.
[22] Steefel CI, DePaolo DJ, Lichtner PC. Reactive transport modeling: An essential tool and a new research approach for the Earth sciences. Earth Planet Sci Lett 2005;240:539–58. doi:10.1016/j.epsl.2005.09.017.
[23] Li L, Salehikhoo F, Brantley SL, Heidari P. Spatial zonation limits magnesite dissolution in porous media. Geochim Cosmochim Acta 2014;126:555–73. doi:10.1016/j.gca.2013.10.051.
[24] Li L, Steefel CI, Kowalsky MB, Englert A, Hubbard SS. Effects of physical and geochemical heterogeneities on mineral transformation and biomass accumulation during biostimulation experiments at Rifle, Colorado. J Contam Hydrol 2010;112:45–63. doi:10.1016/j.jconhyd.2009.10.006.
[25] Chen J, Hubbard SS, Williams KH. Data-driven approach to identify field-scale biogeochemical transitions using geochemical and geophysical data and hidden Markov models: Development and application at a uranium-contaminated aquifer. Water Resour Res 2013;49:6412–24. doi:10.1002/wrcr.20524.

[26] Chen J, Hubbard SS, Williams KH, Flores Orozco A, Kemna A. Estimating the spatiotemporal distribution of geochemical parameters associated with biostimulation using spectral induced polarization data and hierarchical Bayesian models: ESTIMATING GEOCHEMICAL PARAMETERS USING SIP DATA. Water Resour Res 2012;48:n/a – n/a. doi:10.1029/2011WR010992.
[27] Flores Orozco A, Williams KH, Long PE, Hubbard SS, Kemna A. Using complex resistivity imaging to infer biogeochemical processes associated with bioremediation of an uranium-contaminated aquifer. J Geophys Res Biogeosciences 2011;116:G03001. doi:10.1029/2010JG001591.
[28] Hubbard SS, Williams K, Conrad ME, Faybishenko B, Peterson J, Chen J, et al. Geophysical Monitoring of Hydrological and Biogeochemical Transformations Associated with Cr(VI) Bioremediation. Environ Sci Technol 2008;42:3757–65. doi:10.1021/es071702s.
[29] Scheibe TD, Fang Y, Murray CJ, Roden EE, Chen J, Chien Y-J, et al. Transport and biogeochemical reaction of metals in a physically and chemically heterogeneous aquifer. Geosphere 2006;2:220–35. doi:10.1130/GES00029.1.
[30] Williams KH, Kemna A, Wilkins MJ, Druhan J, Arntzen E, N'Guessan AL, et al. Geophysical Monitoring of Coupled Microbial and Geochemical Processes During Stimulated Subsurface Bioremediation. Environ Sci Technol 2009;43:6717–23. doi:10.1021/es900855j.
[31] Williams KH, Ntarlagiannis D, Slater LD, Dohnalkova A, Hubbard SS, Banfield JF. Geophysical Imaging of Stimulated Microbial Biomineralization. Environ Sci Technol 2005;39:7592–600. doi:10.1021/es0504035.
[32] Sassen DS, Hubbard SS, Bea SA, Chen J, Spycher N, Denham ME. Reactive facies: An approach for parameterizing field-scale reactive transport models using geophysical methods. Water Resour Res 2012;48:W10526. doi:10.1029/2011WR011047.
[33] Wainwright HM, Chen J, Sassen DS, Hubbard SS. Bayesian hierarchical approach and geophysical data sets for estimation of reactive facies over plume scales. Water Resour Res 2014;50:4564–84. doi:10.1002/2013WR013842.
[34] Cardiff M, Kitanidis PK. Fitting Data Under Omnidirectional Noise: A Probabilistic Method for Inferring Petrophysical and Hydrologic Relations. Math Geosci 2010;42:877–909. doi:10.1007/s11004-010-9301-x.
[35] Smith E, Naidu R, Alston AM. Arsenic in the Soil Environment: A Review. In: Sparks DL, editor. Adv. Agron., vol. 64, Academic Press; 1998, p. 149–95.
[36] Smedley PL, Kinniburgh DG. A review of the source, behaviour and distribution of arsenic in natural waters. Appl Geochem 2002;17:517–68. doi:10.1016/S0883-2927(02)00018-5.
[37] Fendorf S, Nico PS, Kocar BD, Masue Y, Tufano KJ. Chapter 12 - Arsenic Chemistry in Soils and Sediments. In: Gräfe BS and M, editor. Dev. Soil Sci., vol. 34, Elsevier; 2010, p. 357–78.
[38] Borch T, Kretzschmar R, Kappler A, Cappellen PV, Ginder-Vogel M, Voegelin A, et al. Biogeochemical Redox Processes and their Impact on Contaminant Dynamics. Environ Sci Technol 2010;44:15–23. doi:10.1021/es9026248.
[39] Haberer CM, Rolle M, Cirpka OA, Grathwohl P. Oxygen Transfer in a Fluctuating Capillary Fringe. Vadose Zone J 2012;11:vzj2011.0056. doi:10.2136/vzj2011.0056.
[40] Kocar BD, Polizzotto ML, Benner SG, Ying SC, Ung M, Ouch K, et al. Integrated biogeochemical and hydrologic processes driving arsenic release from shallow sediments to groundwaters of the Mekong delta. Appl Geochem 2008;23:3059–71. doi:10.1016/j.apgeochem.2008.06.026.

[41] Farnsworth CE, Hering JG. Inorganic geochemistry and redox dynamics in bank filtration settings. Environ Sci Technol 2011;45:5079–87. doi:10.1021/es2001612.
[42] Polizzotto ML, Kocar BD, Benner SG, Sampson M, Fendorf S. Near-surface wetland sediments as a source of arsenic release to ground water in Asia. Nature 2008;454:505–8. doi:10.1038/nature07093.
[43] Stuckey JW, Schaefer MV, Benner SG, Fendorf S. Reactivity and speciation of mineral-associated arsenic in seasonal and permanent wetlands of the Mekong Delta. Geochim Cosmochim Acta 2015;171:143–55. doi:10.1016/j.gca.2015.09.002.
[44] Postma D, Larsen F, Minh Hue NT, Duc MT, Viet PH, Nhan PQ, et al. Arsenic in groundwater of the Red River floodplain, Vietnam: Controlling geochemical processes and reactive transport modeling. Geochim Cosmochim Acta 2007;71:5054–71. doi:10.1016/j.gca.2007.08.020.
[45] Frohne T, Rinklebe J, Diaz-Bone RA, Du Laing G. Controlled variation of redox conditions in a floodplain soil: Impact on metal mobilization and biomethylation of arsenic and antimony. Geoderma 2011;160:414–24. doi:10.1016/j.geoderma.2010.10.012.
[46] Molinari A, Ayora C, Marcaccio M, Guadagnini L, Sanchez-Vila X, Guadagnini A. Geochemical modeling of arsenic release from a deep natural solid matrix under alternated redox conditions. Environ Sci Pollut Res 2013;21:1628–37. doi:10.1007/s11356-013-2054-6.
[47] Mirecki JE, Bennett MW, López-Baláez MC. Arsenic control during aquifer storage recovery cycle tests in the Floridan Aquifer. Ground Water 2013;51:539–49. doi:10.1111/j.1745-6584.2012.01001.x.
[48] Prommer H, Stuyfzand PJ. Identification of Temperature-Dependent Water Quality Changes during a Deep Well Injection Experiment in a Pyritic Aquifer. Environ Sci Technol 2005;39:2200–9. doi:10.1021/es0486768.
[49] Vanderzalm JL, Dillon PJ, Barry KE, Miotlinski K, Kirby JK, Le Gal La Salle C. Arsenic mobility and impact on recovered water quality during aquifer storage and recovery using reclaimed water in a carbonate aquifer. Appl Geochem 2011;26:1946–55. doi:10.1016/j.apgeochem.2011.06.025.
[50] Wallis I, Prommer H, Simmons CT, Post V, Stuyfzand PJ. Evaluation of Conceptual and Numerical Models for Arsenic Mobilization and Attenuation during Managed Aquifer Recharge. Environ Sci Technol 2010;44:5035–41. doi:10.1021/es100463q.
[51] Kitanidis PK, Lee J. Principal Component Geostatistical Approach for large-dimensional inverse problems. Water Resour Res 2014;50:5428–43. doi:10.1002/2013WR014630.
[52] Harbaugh AW, Banta ER, Hill MC, McDonald MG. MODFLOW-2000, The U.S. Geological Survey Modular Ground-Water Model - User Guide to Modularization Concepts and the Ground-Water Flow Process. United States Geological Survey; 2000.
[53] Prommer H, Barry DA, Zheng C. MODFLOW/MT3DMS-based reactive multicomponent transport modeling. Ground Water 2003;41:247–57.
[54] Parkhurst D, Appelo C. User's guide to PHREEQC - A computer program for speciation, reaction-path, ID-transport, and inverse geochemical calculations. U.S. Geological Survey Water Resources Investigations Report; 1999.
[55] Fiori A, Jankovic I, Dagan G. The impact of local diffusion upon mass arrival of a passive solute in transport through three-dimensional highly heterogeneous aquifers. Adv Water Resour 2011;34:1563–73. doi:10.1016/j.advwatres.2011.08.010.
[56] Kitanidis PK. The concept of the Dilution Index. Water Resour Res 1994;30:2011–26. doi:10.1029/94WR00762.
[57] Hochstetler DL, Rolle M, Chiogna G, Haberer CM, Grathwohl P, Kitanidis PK. Effects of compound-specific transverse mixing on steady-state reactive plumes: Insights from

686 pore-scale simulations and Darcy-scale experiments. Adv Water Resour 2013;54:1–10.
687 doi:10.1016/j.advwatres.2012.12.007.
688 [58] Rolle M, Chiogna G, Hochstetler DL, Kitanidis PK. On the importance of diffusion and
689 compound-specific mixing for groundwater transport: An investigation from pore to
690 field scale. J Contam Hydrol 2013;153:51–68. doi:10.1016/j.jconhyd.2013.07.006.
691 [59] Rolle M, Kitanidis PK. Effects of compound-specific dilution on transient transport and
692 solute breakthrough: A pore-scale analysis. Adv Water Resour 2014;71:186–99.
693 doi:10.1016/j.advwatres.2014.06.012.
694 [60] Rolle M, Eberhardt C, Chiogna G, Cirpka OA, Grathwohl P. Enhancement of dilution and
695 transverse reactive mixing in porous media: Experiments and model-based
696 interpretation. J Contam Hydrol 2009;110:130–42.
697 doi:10.1016/j.jconhyd.2009.10.003.
698 [61] Prommer H, Tuxen N, Bjerg PL. Fringe-Controlled Natural Attenuation of Phenoxy
699 Acids in a Landfill Plume: Integration of Field-Scale Processes by Reactive Transport
700 Modeling. Environ Sci Technol 2006;40:4732–8. doi:10.1021/es0603002.
701 [62] Prommer H, Anneser B, Rolle M, Einsiedl F, Griebler C. Biogeochemical and Isotopic
702 Gradients in a BTEX/PAH Contaminant Plume: Model-Based Interpretation of a High-
703 Resolution Field Data Set. Environ Sci Technol 2009;43:8206–12.
704 doi:10.1021/es901142a.
705 [63] Price RE, Pichler T. Abundance and mineralogical association of arsenic in the
706 Suwannee Limestone (Florida): Implications for arsenic release during water–rock
707 interaction. Chem Geol 2006;228:44–56. doi:10.1016/j.chemgeo.2005.11.018.
708 [64] Wallis I, Prommer H, Pichler T, Post V, B. Norton S, Annable MD, et al. Process-Based
709 Reactive Transport Model To Quantify Arsenic Mobility during Aquifer Storage and
710 Recovery of Potable Water. Environ Sci Technol 2011;45:6924–31.
711 doi:10.1021/es201286c.
712 [65] Descourvieres C, Prommer H, Oldham C, Greskowiak J, Hartog N. Kinetic Reaction
713 Modeling Framework for Identifying and Quantifying Reductant Reactivity in
714 Heterogeneous Aquifer Sediments. Environ Sci Technol 2010;44:6698–705.
715 doi:10.1021/es101661u.
716 [66] Williamson MA, Rimstidt JD. The kinetics and electrochemical rate-determining step of
717 aqueous pyrite oxidation. Geochim Cosmochim Acta 1994;58:5443–54.
718 doi:10.1016/0016-7037(94)90241-0.
719 [67] Eckert P, Appelo C a. J. Hydrogeochemical modeling of enhanced benzene, toluene,
720 ethylbenzene, xylene (BTEX) remediation with nitrate. Water Resour Res 2002;38:5–
721 1. doi:10.1029/2001WR000692.
722 [68] Kolker A, Haack SK, Cannon WF, Westjohn DB, Kim M-J, Nriagu J, et al. Arsenic in
723 southeastern Michigan. In: Welch AH, Stollenwerk KG, editors. Arsen. Ground Water,
724 Springer US; 2003, p. 281–94.
725 [69] Dzombak DA, Morel FMM. Surface complexation modeling: Hydrous ferric oxide.
726 Wiley, New York; 1990.
727 [70] Fendorf S, Herbel M, Tufano K, Kocar BD. Biogeochemical Processes Controlling the
728 Cycling of Arsenic in Soils and Sediments. Biophys.-Chem. Process. Heavy Met. Met.
729 Soil Environ., John Wiley & Sons; 2007.
730 [71] Dixit S, Hering JG. Comparison of arsenic(V) and arsenic(III) sorption onto iron oxide
731 minerals: implications for arsenic mobility. Environ Sci Technol 2003;37:4182–9.
732 [72] Appelo CAJ, Van Der Weiden MJJ, Tournassat C, Charlet L. Surface Complexation of
733 Ferrous Iron and Carbonate on Ferrihydrite and the Mobilization of Arsenic. Environ
734 Sci Technol 2002;36:3096–103. doi:10.1021/es010130n.

[73] Manning BA, Fendorf SE, Bostick B, Suarez DL. Arsenic(III) Oxidation and Arsenic(V) Adsorption Reactions on Synthetic Birnessite. Environ Sci Technol 2002;36:976–81. doi:10.1021/es0110170.
[74] Scott MJ, Morgan JJ. Reactions at Oxide Surfaces. 1. Oxidation of As(III) by Synthetic Birnessite. Environ Sci Technol 1995;29:1898–905. doi:10.1021/es00008a006.
[75] Ying SC, Kocar BD, Griffis SD, Fendorf S. Competitive Microbially and Mn Oxide Mediated Redox Processes Controlling Arsenic Speciation and Partitioning. Environ Sci Technol 2011;45:5572–9. doi:10.1021/es200351m.
[76] Kitanidis PK. Quasi-Linear Geostatistical Theory for Inversing. Water Resour Res 1995;31:2411–9. doi:10.1029/95WR01945.
[77] Kitanidis PK. On the geostatistical approach to the inverse problem. Adv Water Resour 1996;19:333–42. doi:10.1016/0309-1708(96)00005-X.
[78] Box GEP, Cox DR. An Analysis of Transformations. J R Stat Soc Ser B Methodol 1964;26:211–52.
[79] Snodgrass MF, Kitanidis PK. A geostatistical approach to contaminant source identification. Water Resour Res 1997;33:537–46. doi:10.1029/96WR03753.
[80] Kitanidis PK, Shen K-F. Geostatistical interpolation of chemical concentration. Adv Water Resour 1996;19:369–78. doi:10.1016/0309-1708(96)00016-4.
[81] Haberer CM, Rolle M, Cirpka OA, Grathwohl P. Oxygen transfer in a fluctuating capillary fringe. Vadose Zone J 2012; doi:10.2136/vzj2011.0056.
[82] Haberer CM, Muniruzzaman M, Grathwohl P, Rolle M. Diffusive–Dispersive and Reactive Fronts in Porous Media. IronII Oxid Unsaturated–Saturated Interface. Vadose Zone J 2015. doi:10.2136/vzj2014.07.0091.
[83] Haberer CM, Rolle M, Cirpka OA, Grathwohl P. Impact of heterogeneity on oxygen transport in a fluctuating capillary fringe. Groundwater 2015; doi:10.1111/gwat.12149.
[84] Rolle M, Chiogna G, Bauer R, Griebler C, Grathwohl P. Isotopic Fractionation by Transverse Dispersion: Flow-through Microcosms and Reactive Transport Modeling Study. Environ Sci Technol 2010;44:6167–73. doi:10.1021/es101179f.
[85] Vieweg M, Trauth N, Fleckenstein JH, Schmidt C. Robust Optode-Based Method for Measuring in Situ Oxygen Profiles in Gravelly Streambeds. Environ Sci Technol 2013;47:9858–65. doi:10.1021/es401040w.
[86] Kitanidis PK. Introduction to Geostatistics: Applications in Hydrogeology. Cambridge University Press; 1997.
[87] Kitanidis PK. Orthonormal residuals in geostatistics: Model criticism and parameter estimation. Math Geol 1991;23:741–58. doi:10.1007/BF02082534.
[88] Jones GW, Pichler T. Relationship between Pyrite Stability and Arsenic Mobility During Aquifer Storage and Recovery in Southwest Central Florida. Environ Sci Technol 2007;41:723–30. doi:10.1021/es061901w.
[89] Lazareva O, Druschel G, Pichler T. Understanding arsenic behavior in carbonate aquifers: Implications for aquifer storage and recovery (ASR). Appl Geochem 2015;52:57–66. doi:10.1016/j.apgeochem.2014.11.006.